A novel bioactive polyurethane with controlled degradation and L-Arg release used as strong adhesive tissue patch for hemostasis and promoting wound healing

Faxing Zou [a], Yansen Wang [a], Yudong Zheng [a,*], Yajie Xie [a], Hua Zhang [b,**], Jishan Chen [a], M. Irfan Hussain [a], Haoye Meng [c], Jiang Peng [c,***]

[a] School of Material Science & Engineering, University of Science and Technology Beijing, Beijing, 10083, China
[b] The First Affiliated Hospital of Chongqing Medical University, China
[c] Beijing Key Lab of Regenerative Medicine in Orthopedics, Key Laboratory of Musculoskeletal Trauma & War Injuries, PLA Institute of Orthopedics, Chinese PLA General Hospital, Beijing, China

ARTICLE INFO

ABSTRACT

Effective strategy of hemostasis and promoting angiogenesis are becoming increasingly urgent in modern medicine due to millions of deaths caused by tissue damage and inflammation. The tissue adhesive has been favored as an optimistic and efficient path to stop bleeding, while, current adhesive presents limitations on wound care or potential degradation safety in clinical practice. Therefore, it is of great clinical significance to construct multifunctional wound adhesive to address the issues. Based on pro-angiogenic property of L-Arginine (L-Arg), in this study, the novel tissue adhesive (G-DLPUs) constructed by L-Arg-based degradable polyurethane (DLPU) and GelMA were prepared for wound care. After systematic characterization, we found that the G-DLPUs were endowed with excellent capability in shape-adaptive adhesion. Moreover, the L-Arg released and the generation of NO during degradation were verified which would enhance wound healing. Following the in vivo biocompatibility was verified, the hemostatic effect of the damaged organ was tested using a rat liver hemorrhage model, from which reveals that the G-DLPUs can reduce liver bleeding by nearly 75% and no obvious inflammatory cells observed around the tissue. Moreover, the wound care effect was confirmed in a mouse full-thickness skin defect model, showing that the hydrogel adhesive significantly improves the thickness of newly formed dermis and enhance vascularization (CD31 staining). In summary, the G-DLPUs are promising candidate to act as multifunctional wound care adhesive for both damaged organ and trauma.

1. Introduction

Hemostasis and enhancing wound healing are important issues in tissue repair, and have become an urgent issue and have attracted increased attention in recent years [1,2]. It is reported that uncontrollable bleeding and wound infection lead to a high mortality rate in the world and cause more than millions of deaths each year [3]. Studies demonstrate that rapid wound closure and enhancing wound healing can effectively reduce mortality [4]. Inevitably, when the tissue damaged, the blood vessel tissue will be destroyed, which will increase the difficulty of hemostasis and tissue repair. Blood vessels (BVs) present all over human tissue and act as an indispensable role in the body, vascularization of the wound tissue is one of the important symbols of wound healing.

Previous reports on tissue wound adhesive tend to focus on adhesion, and degradability of the material [5], while the enhancement of skin healing process and the regeneration of BVs are less investigated, and few wound adhesives with multifunction of adhesion to hemostasis, BVs growth promotion and degradation safety are reported [6–8]. Hence, it is of clinical significance to construct versatile wound adhesive for

addressing these problems [9–11].

L-arginine (L-Arg), a pivotal mediator during the wound healing process [12], could be catalyzed into nitric oxygen (NO) and ornithine by nitric oxide synthase (NOS) and arginase at the wound site, respectively. Additionally, the NO derived from L-Arg acts as an important role to antibacterial and anti-inflammatory and promote angiogenesis. Besides, as a precursor for proline synthesis, the ornithine accelerates wound healing by contributing itself as a substrate for the synthesis of collagen [13]. Therefore, L-Arg has become a popular supplement for promoting wound healing [14]. However, it is inefficient for patients to take it orally, because it fails to concentrate locally on the wound tissue [15]. Therefore, more and more composites were developed to deliver L-Arg locally and directly in damaged tissue. Nevertheless, the previous studies cannot be blind at the sharp and random release of L-Arg on the wound. There are many side effects that has been confirmed that the excessive L-Arg would have a disadvantage to the activity of ornithine-decarboxylase [16] and prompt the formation of scar and fibrosis [17]. It is of particular importance to construct a slow release strategy of L-Arg for wound healing to avoid adverse reactions.

In view of the molecular structure of L-Arg, we construct a waterborne polyurethane (WPU) with adjustable structure as a starting point to design and prepare would adhesive, due to that the PU has excellent biocompatibility and controllable biodegradability which is widely used in the biomedical field [18–20]. Based on the structural adjustability of the PU, the multifunction of tissue adhesion and biodegradation safety were endowed with PU via introducing the active functional groups and segments in the molecular chain [21], such L-Arg, drug-load chain extender β-CD and soft segment PEG.

The degradable polyurethane selected could address the problem attributing to that it possesses excellent biodegradability and biocompatibility, which would release L-Arg during the degradation process. Moreover, constructing a suitable degradable polyurethane structure can endow the material with good biocompatibility and biodegradation safety [11,22], which is a thorny problem that most research on tissue adhesives ignores. The safety of biodegradation enables the material to have excellent degradation properties while avoiding the accumulation of tissue acid and thus inflammation. Furthermore, related studies have shown that it exerts the adhesion through strong hydrogen bonding among molecular, instead of current tissue adhesives, which functionalized using isocyanate (NCO) [23], aldehyde (CHO) [24] or NHS-activated ester [10,25,26], achieving adhesion through chemical bonding, more inclined to release low-molecular compounds, bring about unpredictable harm to the body.

In addition, the release of L-Arg and the realization of adhesion also need to provide adhesion support to vascular endothelial cells. Obtained by modifying gelatin, gelatin-methacryloyl (GelMA) can provide sites for vascular endothelium attachment via RGD (Arg-Gly-Asp) motifs, and create a suitable environment for cell proliferation, differentiation and remodeling [27–29].

Dual-network-structure adhesive with adhering to the wound and releasing L-Arg during the degradation process, which makes it possible to promote healing of the wound. Herein, assuming that a waterborne polyurethane combined with GelMA, the formed composite would possess the function of shape-adaptive adhesive capability, and could be adhere to the wound and achieve hemostasis, while the polyurethane and GelMA can release the amino acid and RGD peptides during degradation process. Under this consideration, we constructed a multifunctional wound adhesive composed of L-Arg-based waterborne polyurethane compounded and gelatin methacryloyl (GelMA) (Fig. 1). This hydrogel can provide a moist recovery environment for the wound and a suitable environment for cells to adhere and grow. Meanwhile, the adhesive has the function to enhance blood vessel regeneration and wound healing through the release of L-Arginine during the degradation process (Fig. 8). The effectiveness of this wound adhesive (G-DLPU3) in biodegradability in vivo, organ damage hemostasis and wound care were investigated successively by rat subcutaneous implantation experiment,

rat liver hemorrhage model and mouse full-thickness skin defect model. The synergistic activity of the materials in composite was verified and revealed that the hydrogel adhesive significantly improves the new skin tissue thickness and enhances vascularization, making it a promising candidate to use as multifunctional wound adhesive for hemostasis and promotion of wound healing.

2. Experimental section

2.1. Materials

Polyethylene glycol (PEG, Mn = 400), L-Arginine (L-Arg), β-Cyclodextrin (β-CD) were obtained from China Sinopharm Group Reagent Co, Ltd. Isophorone diisocyanate (IPDI), Gelatin, Type A and Methacrylic anhydride (MA) were obtained from Sigma-Aldrich (Shanghai, China). Stannous caprylate, dimethylol propionic acid (DMPA) were bought from Alfa Aesar Corporation (Shanghai, China). Other raw materials such as acetone and triethyl amine (TEA) were obtained from Kelong Chemical Corporation (Chengdu, China), and used without further purification. Hoechst33342 was purchased from Leagene Biotech Co., Ltd. (Beijing, China). The Calcein AM was obtained from Shanghai yaji biotechnology Co., Ltd. (Shanghai, China). The CCK-8 kit was obtained from Dojindo (Japan).

2.2. Preparation of DLPU, GelMA and G-DLPUs

2.2.1. Preparation of DLPU

The preparation process of carboxyl-rich (DMPA) amino acid (L-Arg) modified polyurethane is shown as follows: Equipping with nitrogen gas inlet, thermometer and stirrer, the flask was fixed on the oil bath, and the raw materials such as soft Polyethylene glycol and chain extender β-Cyclodextrin (β-CD) were successively added at temperature of 90 °C and stirred for 1 h to make them homogeneous. In the nitrogen atmosphere, after adding catalyst, the total IPDI (-OH/-NCO = 0.5) was added intermittently into stirred flask, then the reaction was performed at 80 °C for 3 h. Setting the temperature to 75 °C, the dissolved DMPA solution was dropped into the flask and reacted for another 1.5 h. After the prepolymerization, the obtained NCO-terminated prepolymer was cooled to below 50 °C and appropriate amount of acetone was used to adjust the viscosity of the prepolymer. Then, the TEA was used to neutralize the carboxylic acids in the DMPA to improve the solubility of polymer. The solution containing 0.5 g L-Arg was added dropwise to neutralize the isocyanate group of prepolymer and maintained vigorous mechanical stirring at 1000 rpm for 0.5 h to obtain solution. The prepared tissue adhesive DMPA and L-Arg modified polyurethane named DLPU.

2.2.2. Preparation of the GelMA

GelMA was synthesized using methods as depicted in Fig. 1b. Briefly, under constant magnetic stirring, the type-A gelatin was dissolved in 50 ml Dulbecco's phosphate buffered saline (DPBS) at 60 °C. All methacrylic anhydride was continuously added to the solution within 10 min, and excessive DPBS was poured in to cease the reaction after 3 h of reaction. Subsequently, to remove impurities, the reacted solution was dialyzed in distilled water for 7 days. Finally, the dialyzed solution was subjected to freeze-drying for 48 h to obtain porous modified gelatin (GelMA) which was stored at −20 °C for later use.

The degree of methacryloyl modification was assessed quantifiedly via the ^{1}H NMR spectroscopy (Bruker AV II-400 MHz spectrometer) using the method described by Shirahama et al. [30]. In brief, the proton signal (d = 7.0–7.5 ppm), attributed to aromatic amino acids, was used as a reference in each spectrum. The NMR spectra were integrated over the 2.7–2.9 ppm range, near lysine amino acid, using proton signal from the methylene groups. The degree of substitution (DS) was calculated as following equation:
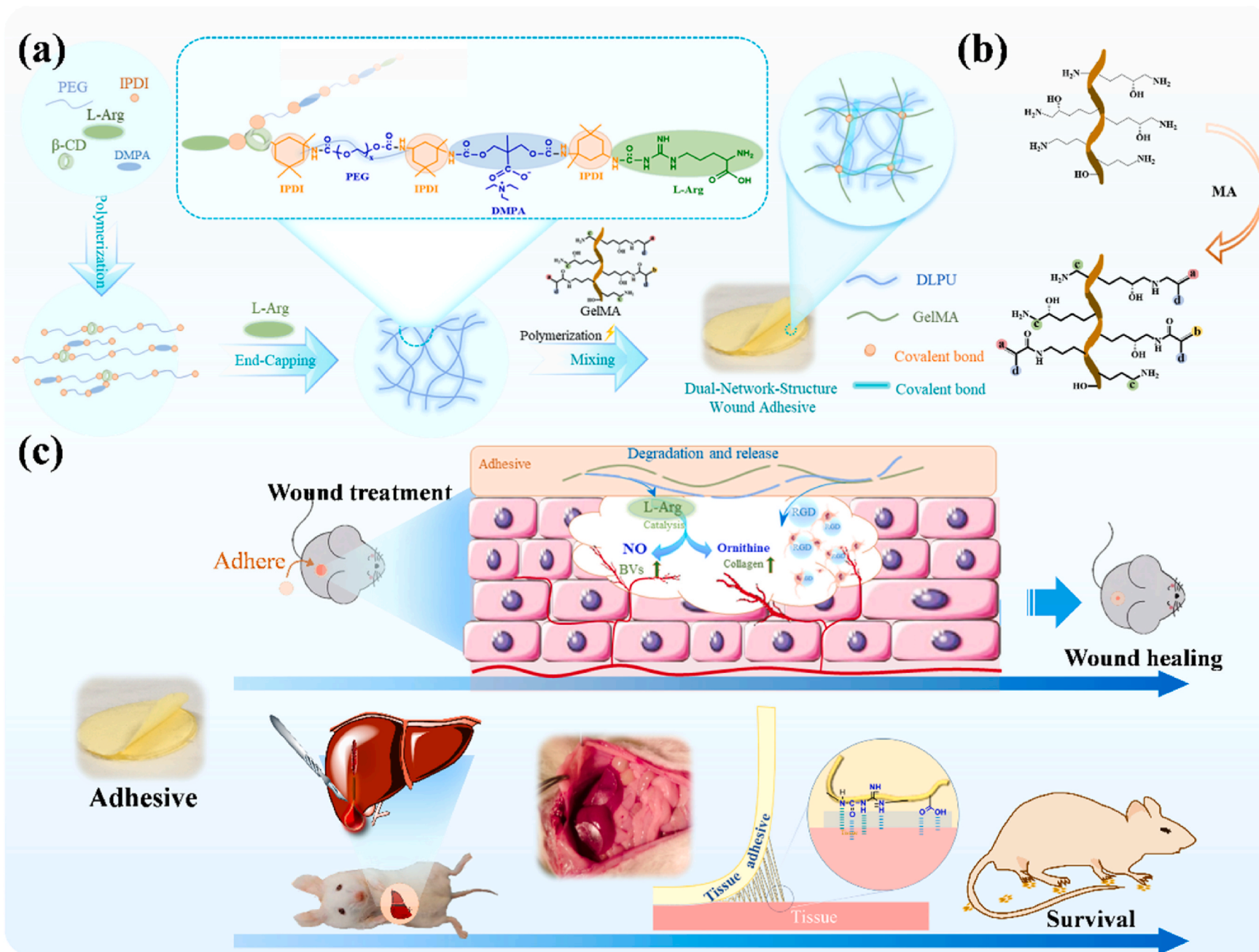
Fig. 1. Schematic representation of the G-DLPUs in construction and application. (a) The construction process of DLPU and G-DLPUs; (b) The synthesis of GelMA; (c) Schematic diagram of the G-DLPUs in promoting angiogenesis and hemostasis.
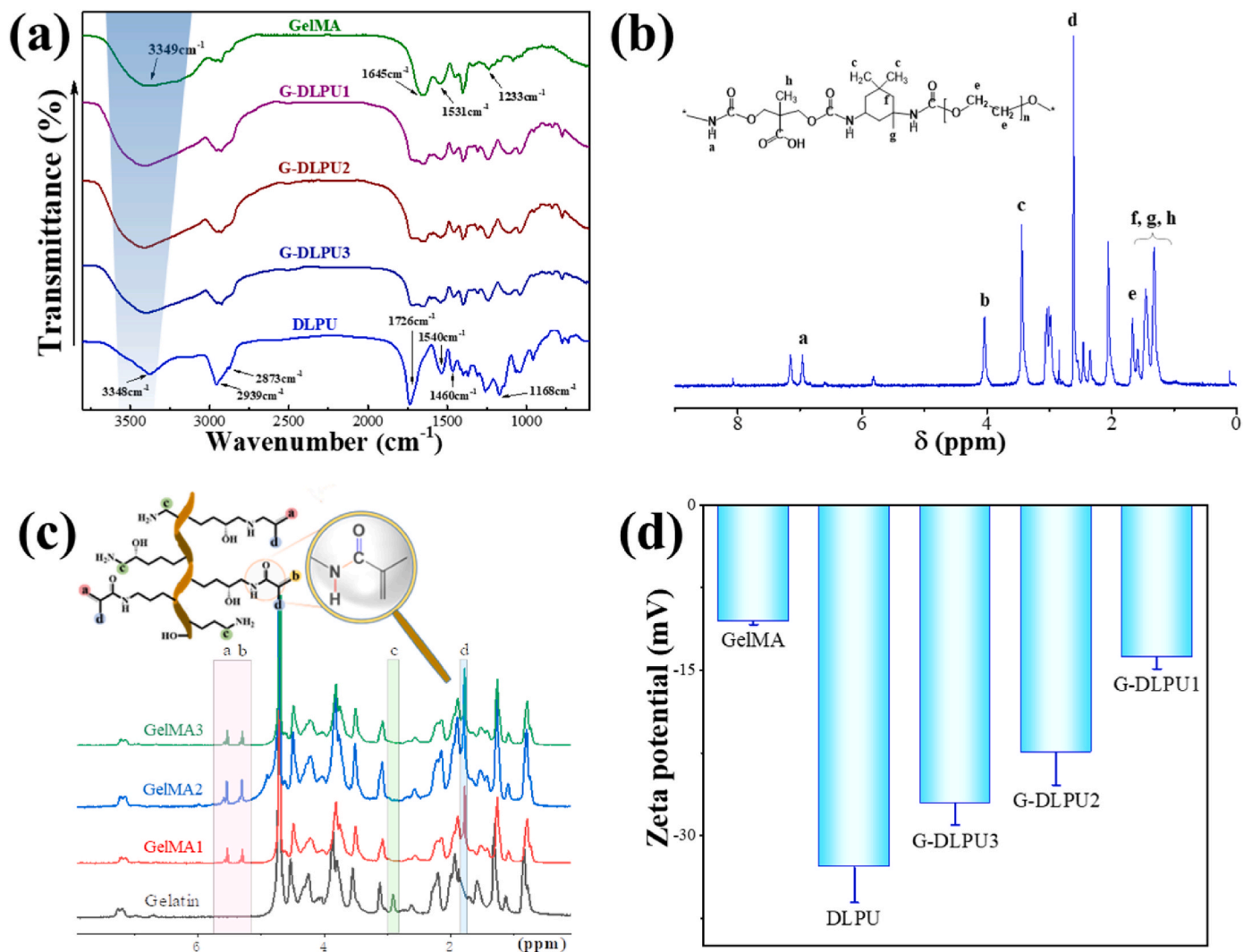
Fig. 2. Characterization of DLPU, GelMA and G-DLPUs. (a) The FT-IR spectra of G-DLPUs; (b) and (c) The ^{1}H NMR spectra of DLPU and GelMA; (d) The zeta potential of G-DLPUs.

$$DS\% = \left(1 - \frac{P_{GelMA}}{P_{gelatin}}\right) \times 100\% \qquad (1)$$

where P_{GelMA} and $P_{gelatin}$ were the peak area of lysine methylene protons in GelMA and gelatin at around 3.0 ppm, respectively.

2.2.3. Preparation of the G-DLPUs

The DLPU solution was obtained by dialysis and concentration prepared above, and the G-DLPUs samples were prepared via the combination of the DLPU and GelMA as shown in Fig. 1c. The GelMA was dissolved in the DLPU concentrated solution (15% w/v) and fully mixed by continuous intense mechanical stirring for 30 min. And after the addition of I2959 photoinitiator (0.5% w/v), the covalent crosslinking structure was formed in GelMA under the 5-min irradiation of ultraviolet light (led light-curing system UPS81, 365 nm, 10 W power). The target composites are coded "G-DLPU#", where "#" is the number representing the mass ratio of DLPU and GelMA. The DSP was prepared as the previous literature [26] using acrylic acid and gelatin with a small amount of crosslinking agent.

2.3. Structural characterization

Rheological tests were conducted to detect the mechanical properties and rheological properties of adhesives using a rheometer (MCR92

Anton Paar, Austria). Amplitude sweeps were performed at a constant frequency of 1 Hz starting from the strain of 1%. The sharply rising storage modulus (G′) was recorded to signify the sol-gel transition of the hydrogel under the interval UV light irradiation, during which the Uv light radiation is every 1 min for 1min.

The chemical structures of hydrogels were tested spectroscopically via Fourier Transform Infrared spectrometer (TENSOR II spectrometer Bruker, Germany) with a resolution of 4 cm^{-1} and frequency range from 4000 cm^{-1}–800 cm^{-1}. With tetramethylsilane (TMS) as an internal standard, the spectrometer (Bruker AV II-400 MHz spectrometer, Switzerland) was used to obtain the ^{1}H NMR spectra of DLPU and GelMA.

The Scanning Electron Microscopy (AURIGA Cross Beam FIB/SEM Station. Carl Zeiss, Germany) was applied to observe the morphology and microstructure of the composites with the accelerating voltage of 15 kV. To increase the resolution, all the dried samples were gold-sputtered prior to imaging.

The Static Contact angle (CA) test was conducted by the contact angle goniometer (OCA20, Dataphysics Inc. Germany) using deionized water at room temperature of 20 °C. In detail, the 2 µL drops of deionized water droplets were dropped on the surface of samples from 10 mm high. After 3 s, the droplets on the sample were photographed, and the contact angle was calculated. Each measurement was performed under the identical experimental conditions. To obtain accurate results, all
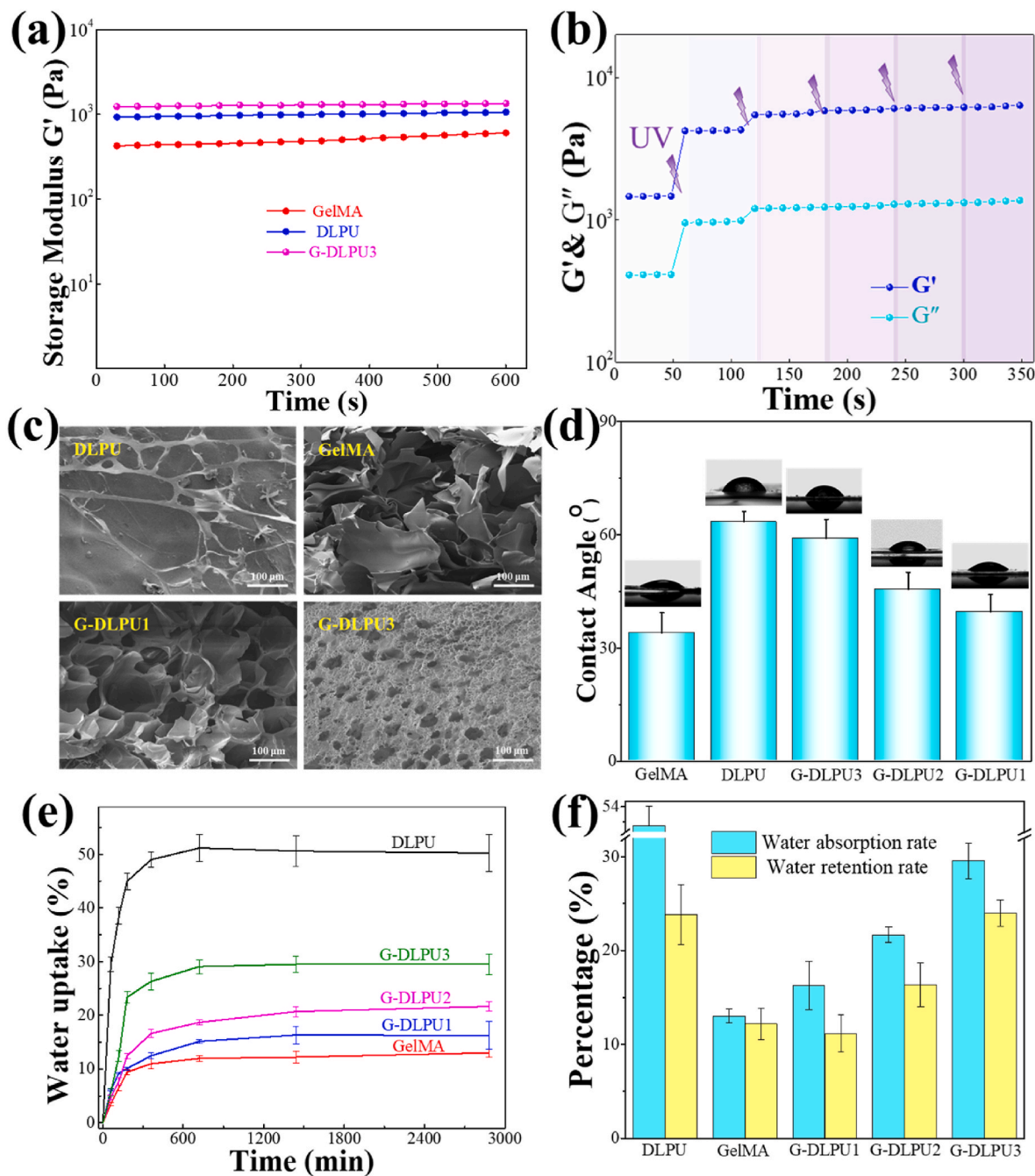
Fig. 3. Characterization of G-DLPUs. (a) The storage modulus of DLPU, GelMA and G-DLPUs; (b) Gelation process of dual network hydrogel (G-DLPU3); (c) The microstructure of the samples; (d) Water contact angle; (e) The absorption curve; (f) water absorption capacity and water retention rate.

samples were tested for three times.

The Coulter LS230 system (USA. Beckman Coulter Inc.) was used to measure the zeta potential of DLPU, GelMA and G-DLPUs solutions at 20 °C. Diluting with water, a few milliliters of dilute solution were prepared to test without further processing. The mean values of zeta potential were calculated after each test was repeated.

2.4. Water absorption and water retention ability

The liquid-absorption rate of the samples in SBF (Simulated Body Fluid) was tested as the following steps: sample was cut into a weight of about 100 mg (W_0) and immersed in SBF (37 °C). The samples were taken out and weighed at different time intervals (1 h, 2 h, 3 h, 6 h, 12 h, 24 h and 48 h). After the extra water on surface was sucked off using

filter paper, the swollen samples were reweighted (W_s). The equation [31] below was used to calculate the liquid-absorption of samples:

$$\text{Water absorption} = \frac{W_s - W_0}{W_0} \times 100\% \tag{2}$$

The liquid-retention abilities of samples were evaluated subsequently. After three samples of each group were immersed in SBF for 24 h, the samples of GelMA, DLPU and G-DLPUs were weighed and recorded (Wd) respectively. After the extra water on surface was sucked off using filter paper, the sample was placed in centrifuge tubes and centrifuged at 800 rmin^{-1} for 3 min. Finally, samples were taken out and reweighted (W_w). Each sample was tested in triplicate. The defined equation following was used to calculate the liquid-retention ratio (W_R) [31]:
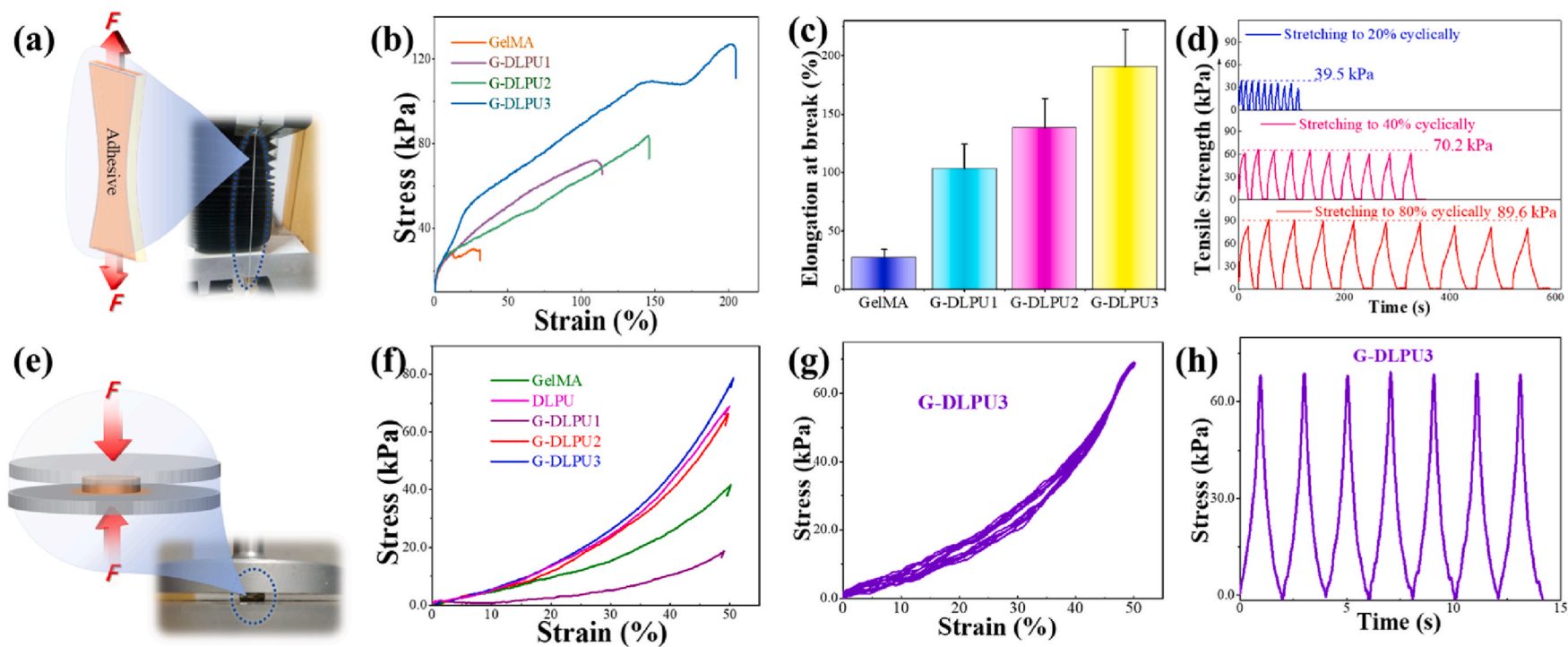
Fig. 4. The mechanical properties. (a) Schematic diagram of tensile properties; (b) The typical tensile stress–strain curves of samples; (c) The elongation at break of G-DLPUs (n = 3); (d) The cyclic tensile properties of G-DLPU3 (20%, 40% and 80%); (e) Schematic diagram of compression performance test; (f) The typical compressive stress–strain curves; (g) and (h) The cyclic compression curve of G-DLPU3.
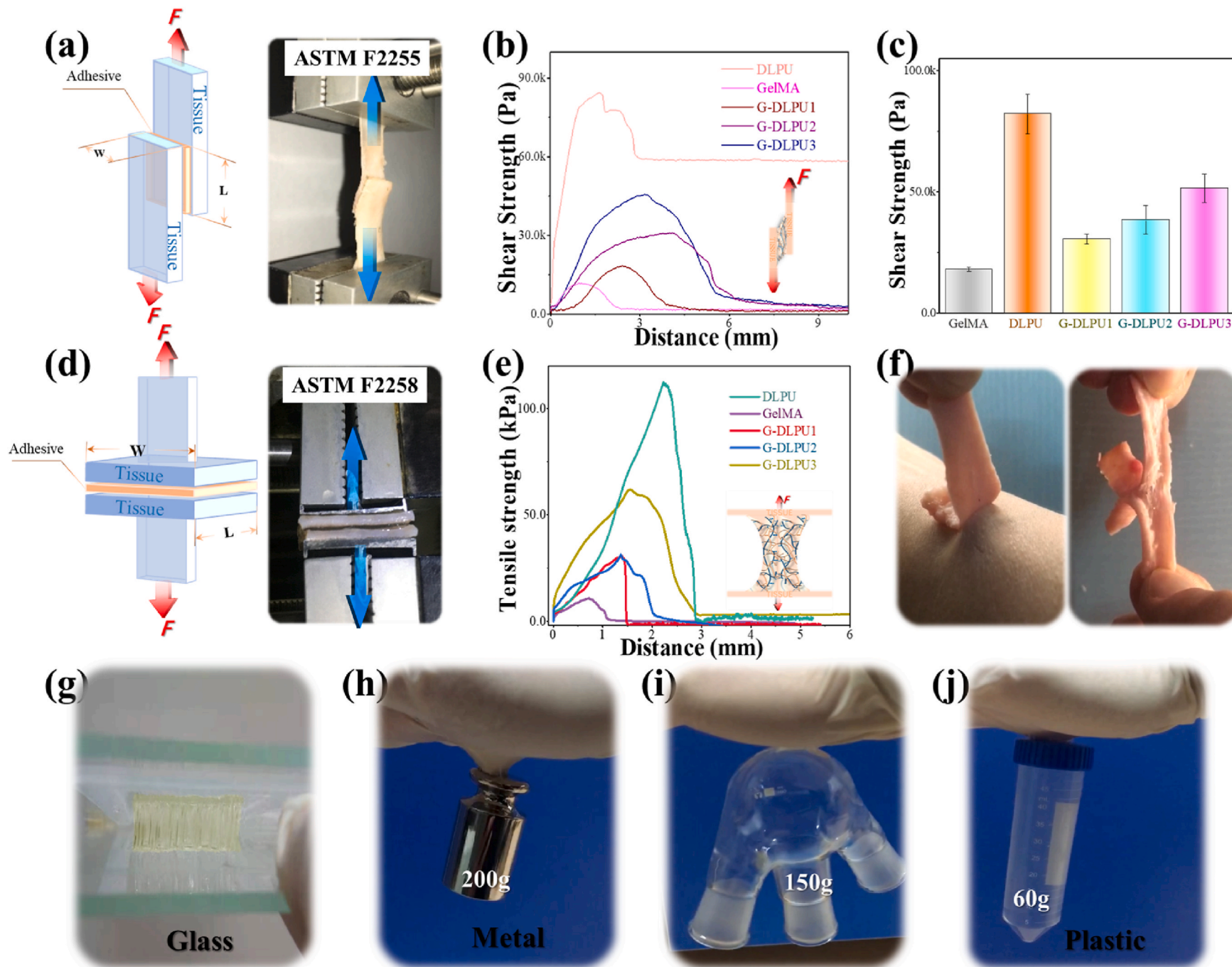
Fig. 5. Evaluation of adhesive behavior; (a) Schematic diagram of shear strength; (b) and (c) The shear strength of G-DLPUs adhesion to porcine skin (n = 3); (d) Schematic diagram of tensile strength; (e) The tensile strength of G-DLPUs adhesion to porcine skin; (f) The G-DLPU3 hydrogel could stick tightly to skin; (g), (h). (i) and (j) The adhesion of G-DLPU3 to flat glass, metal, curved glass and plastic.
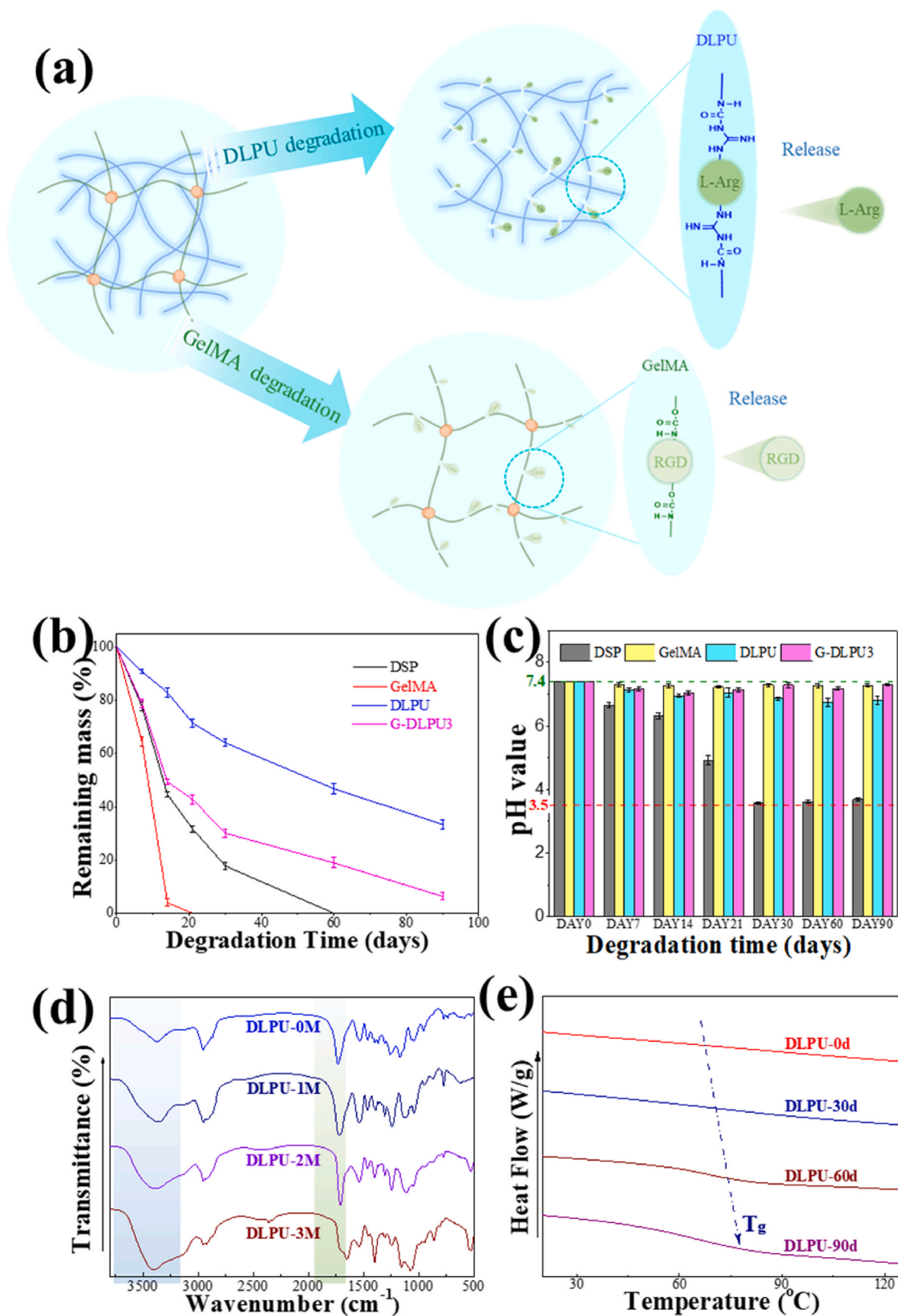
Fig. 6. The biodegradation of DLPU and G-DLPUs; (a) The biodegradation scheme of DLPU; (b) The mass loss curves of biodegradation; (c) The pH value of degradation liquid; (d) and (e) The FTIR spectra and DSC curves of DLPU before and after biodegradation.
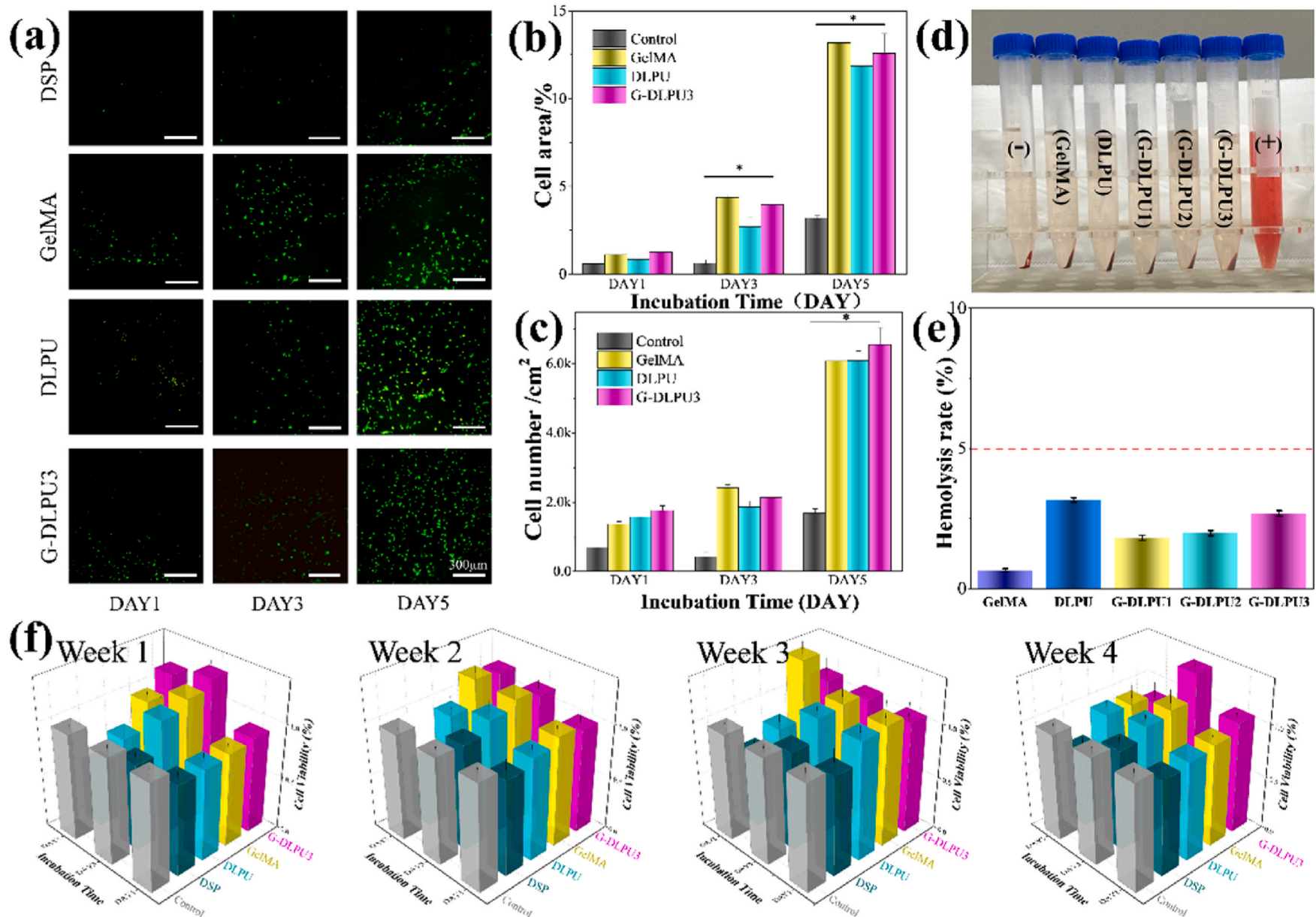
Fig. 7. In vitro biosafety testing. (a) Fluorescence micrographs of NHDF with living cells staining after proliferation on surfaces with DSP, DLPU, GelMA and G-DLPU3 respectively. Statistics of the spreading area (b) and cell density (c) on surfaces of different samples after culturing for 1, 3 and 5 days, Error bars, mean ± s.d. *p < 0.05, represents significant difference compared with blank group (n = 6); (d) and (e) The hemolysis test digital images and hemolysis rate of G-DLPUs. (f) The CCK-8 assay results of cell in the biodegradation solutions.
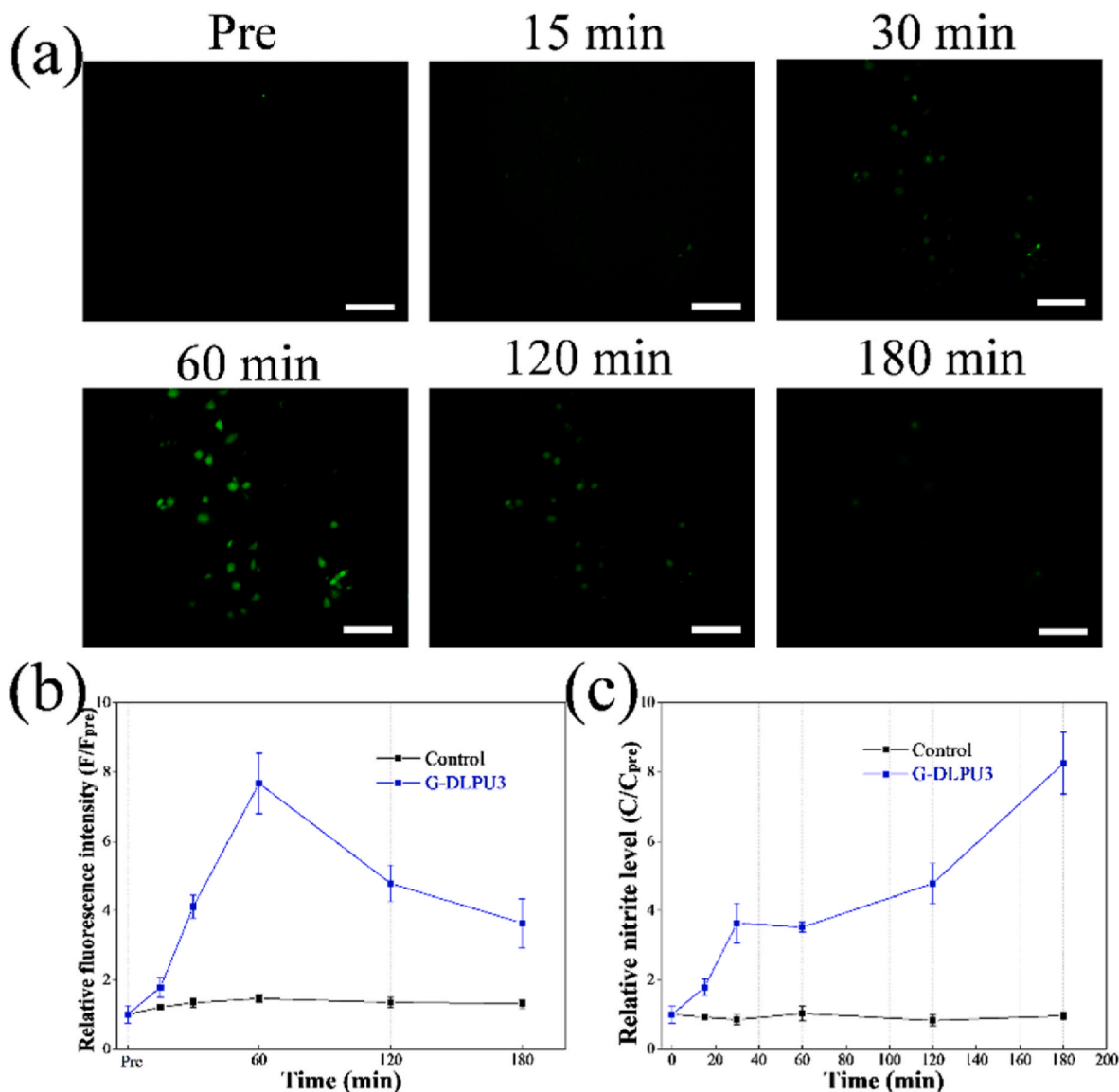
Fig. 8. In vitro characterization of the generation and biological functions of NO. (a) Images of NO production over time in HUVECs stained with DAF-FM DA. scale bar, 50 μm. (b) Calculation of relative fluorescence intensity of NO production in HUVECs; (c) Relative nitrite levels in the culture supernatants measured by the Griess reaction.

$$W_R\% = \frac{W_w - W_0}{W_0} \times 100\% \qquad (3)$$

2.5. Mechanical behavior

The mechanical behaviors including tensile and compression were performed on Texture Analyzer (TA-XT plus, Stable Micro Systems, UK) at a normal temperature of about 25 °C with the speed of 50 mm min^{-1} in stretching and compressing. The original G-DLPUs hydrogels with the size of $40.0 \times 10.0 \times 1.0$ mm was used for the tests and each sample was measured 3 times separately. The cyclic-tensile measurements were performed with the maximum deformation is 20%, 40% and 80% respectively, and stretching 10 times cyclically for each sample.

2.6. Adhesive properties of hydrogels

Adhesive performance of the G-DLPUs was measured via the mechanical testing Texture Analyzer (TAXT plus, Stable Micro Systems, UK), using adhesion test in accordance with ASTM (F2255 and F2258) standards. Details were as follows [2,26]:

Pre-test processing: Adhesive properties of samples were measured using fresh porcine skin which was purchased from the local market and stored at the temperature of −18 °C for later test. To prepare auxiliary materials for testing the adhesion of samples, the porcine skin was taken out and thawed in the PBS solution before being trimmed into rectangular pieces. Subsequently, the well-cut skin was re-immersed to prevent dryness. The rectangular skin was taken out and the surface water was removed carefully and the hydrogel was attached to one end for testing. The samples were then uniformly fitted to the skin surface using a scalpel. A certain amount of pressure was applied to stick it to another piece of skin and adhere firmly.

Shear strength: Each adhered sample was tested using TA-XT plus texture analyzer with an identical adhesion area of 10.0×10.0 mm according to the standard lap-shear test (ASTM F2255) (Fig. S2a). The tensile speed of 50 mm min^{-1} was applied in this test, and the shear strength was determined via dividing the maximum force by the adhesion area.

Tensile strength: Each adhered sample was prepared and tested using TA-XT plus texture analyzer with an identical adhesion area of 20.0×20.0 mm according to the standard lap-shear test (ASTM F2258)

(Fig. S2b). The test was run with a tensile speed of 50 mm min^{-1}. Tensile strength was measured via dividing the maximum force by the adhesion area. Aluminium fixtures were applied, and the tissue was fixed using clips for tensile tests.

Each group of samples was tested multiple times. The shear strength and tensile strength were measured and calculated by the following equations:

$$\text{Shear\ \ strength} = \frac{F_{max}}{WL} \qquad (4)$$

$$\text{Tensile\ \ strength} = \frac{F_{max}}{WL} \qquad (5)$$

The W and L represent the width and length of the adhesion area, respectively.

2.7. The biocompatibility in vitro

2.7.1. Cell compatibility test

To test and evaluate the biocompatibility of samples, we cultured further rat adipose stem cells on the G-DLPUs to observe the attachment and proliferation of cells [32–34]. All materials were treated in ultraviolet-sterilized biosafety cabinet before use. The suspended cells with the concentration of 1×10^5/ml were sow on the sample, and placed in cell incubator after adding the medium. After incubation for 1, 3 and 7d, cells were rinsed with PBS and stained by an Annexin V-FITC/PI cell apoptosis detection kit (Nanjing China) which was applied to view, assess and analyze the growth of cell, following the steps in the instructions. The cells were incubated in the dark for 10min at 37 °C and then viewing under a fluorescent microscope (PUDA FM-600C, China).

2.7.2. Hemocompatibility assay

The hemolysis rate of the DLPU and G-DLPUs were tested according to the following process. In brief, 8 ml of fresh anticoagulant rabbit blood was extracted and diluted with 10 ml of physiological saline; 21 test tubes were divided into the GelMA batch, DLPU batch, G-DLPUs negative control and positive control; The hydrogel with a volume of 0.5 ml was added to the corresponding batch (leaching with 0.9% saline for 72 h, 10 ml); 10 ml of physiological saline was added to the negative control and 10 ml of distilled water was added to the positive control.

All samples were placed in water bath of 37 °C preheated for 60 min, subsequently, the diluted anticoagulant rabbit blood was added into each tube equally, then the tubes were replaced in a 37 °C water bath for 2 h; each tube was centrifuged (2000 r min^{-1}) for 10 min, finally, the supernatant was taken from each tube to measure the absorbance at 545 nm. The absorbance values of each group were recorded from three samples, and the hemolysis rate (H_R) was calculated by the following formula.

$$HR = \frac{A_s - A_n}{A_p - A_n} \times 100\% \qquad (6)$$

where A_p and A_n indicate the absorbance of the positive control and the negative control, respectively, and A_s indicates the absorbance of the samples.

2.7.3. The evaluation of biodegradation safety in vitro

In vitro degradation safety test: To assess the degradation properties [35], the prepared samples ($10 \times 10 \times 1.0$ mm) containing collagenase II and 20 ml PBS were added successively into a container, then shaking constantly at 37 °C. Biodegraded after 7d, 14d, 21d, 30d, 60th and 90th days, the weight loss of the samples was measured after lyophilization. The PH meter (PHS-25, Shanghai INESA Scientific Instrument Co., Ltd, China) was used to determine the pH value of the supernatant, and then the liquid was freeze-dried to characterize degradation products, respectively. Furthermore, to study the cell biocompatibility of the

degrading products produced from the samples, the cell proliferation was detected by performing CCK-8 assay carried out following to manufacturer's advising.

The cell counting Kit-8 (CCK-8) assay: The microplate reader (800 TS Microplate Reader, BioTek Instruments, USA) was used to measure and evaluate the cytotoxic effect of degradation products on cells, and specific steps are as follows [11]. The biodegraded liquid was treated by passing through a 0.2-μm sterilizing filter before use. The rat adipose stem cells (rASC) with the density of 5×10^4 cells per ml were suspended and sown in a culture plate, and the cells could adhere on plate for 12 h in incubator. Then the culture medium was replaced with the mixture of degraded liquid and new cell culture medium. Each well containing cells was washed with PBS buffer several times to flush out the nonadherent cells, after culturing for 1, 3 and 5 days. Hereafter, the CCK-8 reagent was dropped into each well and the plates were shielded from light and incubated at 37 °C for a couple of hours. The microplate reader was used to measure the optical density (OD) values of each well at 450 nm after incubation.

2.8. In vitro NO generation

2.8.1. Release behavior of L-Arg

To reveal the in vitro release behavior of L-Arg from G-DLPU3 during degradation process, several definite concentration purified L-Arg solutions were mixed with the equal volume of 10% ninhydrin solution and measured at 562 nm wavelength using a microplate reader (800 TS Microplate Reader, BioTek Instruments, USA). The purified L-arginine standard curve was determined from the corresponding absorbance versus L-arginine concentration (Fig. S7a). The degradation experiments of G-DLPUs were performed for 1, 2, 3, 5 and 7 days. The degradation liquid was collected and mixed with 10% ninhydrin solution. And then, the mixed solution was measured in triplicate at 562 nm wavelength using the microplate reader. The L-Arg concentration was determined by correlation to standard curve [36].

2.8.2. The NO generation by L-Arg in vitro

For evaluating NO generation in Human Umbilical Vein Endothelial Cells (HUVECs), the NO fluorescent probe DAF-FM DA (Beyotime Biotechnology, Haimen, China) was added into the cells at the concentration of 3 μM. After incubation in cell incubator for 30 min [36], the redundant probe was wash away using PBS. A 50 μL amount of degradation liquid was added into the petri dish (v/v = 9:1). And then the fluorescent microscope (PUDA FM-600C, China) was applied to monitor the NO generation at different time points. The ImageJ software was used to quantify the fluorescence intensity of the captured images.

The Griess reaction was applied to monitor the nitrite level of the culture supernatant [36]. The NO detection kit (Beyotime Biotechnology, Haimen, China) was applied to measure the nitrite level, and the corresponding absorbance was recorded at 490 nm using the microplate reader (800 TS Microplate Reader, BioTek Instruments, USA).

2.9. In vivo experiments

All animal experiments were approved by Institutional Animal Care and Use Committee of Chinese PLA General Hospital. Prior to testing, all the samples were sterilized by cobalt-60 radiation.

Liver injury model: According to the method of literature, a hemorrhaging liver model [2,37] of Sprague Dawley (SD) rat (8–12 weeks, 250 g, male) was used to assess the hemostatic efficiency of G-DLPU3. Briefly, after the anesthetic (isoflurane) was injected in each rat at 60 mg per kilogram, the rats were anesthetized and placed on the pad. The abdomen of rat was gently opened using scalpel to expose the liver, and the intestine was covered by sterilized moistened gauze to keep moist. Before the pre-weighted filter paper was placed under the liver, lightly wipe away remaining fluid on the liver. A 10-mm surgical incision was created on the liver of each rat, then the wound of group was treated

with G-DLPU3, another group treating nothing was named as a control group. Three minutes later, the filter paper absorbing blood oozing from the liver was weighed respectively. The temperature of rats was maintained using heating pad during surgery, and the rat all survived after the experiment. All procedures above were following the Beijing Municipal Regulations on Ethics of Laboratory Animals.

Full-Thickness Wound Healing Study: Male BALB/c mice (6–8 weeks old) provided by Chinese PLA General Hospital and housed at a constant temperature. After the mice were anesthetized with 1.5% isoflurane, a 10 mm diameter full thickness skin round wounds were created on the dorsal skin. The mouse was divided into two groups randomly, control group (n = 9) and G-DLPU3 group (n = 9). The G-DLPU3 group was treated with the sterilized G-DLPU3 samples, while, all controls were covered with sterile gauze directly. The wounds were captured by a digital camera at the predetermined time intervals, and the wound area were calculated by the ImageJ program. The tissues around the wound were dissected, and the H&E staining and immuno-histochemical analysis (CD31 expression) were carried out according to standard protocols. The number and diameter of new blood vessels on day 14 were determined averagely by counting three areas of the CD31 staining using ImageJ program.

2.10. Statistical analysis

All values results were expressed as a mean ± standard deviation (SD) and statistical analysis was determined using one-way ANOVA. If P < 0.05, the differences were considered statistically significant.

3. Results and discussion

3.1. Physicochemical characterization of hydrogels

3.1.1. Chemical structure and microstructure characterization

The synthetic scheme of DLPU, GelMA and G-DLPUs were depicted in Fig. 1. To verify the successful preparation of DLPU, GelMA and G-DLPUs, the structures of polymers were investigated using FT-IR and ^{1}H NMR (Fig. 2). The FT-IR spectrum of DLPU exhibited vital spectral absorbance features at 3348 cm^{-1}, 1726 cm^{-1}, which respectively assigned to N–H stretching vibration of aliphatic secondary amine and C═O stretching vibration of the esters and carboxyl [22]. In addition, the absorption peaks of N–H bending vibration and C–N stretching vibration [21] of aliphatic secondary amine were observed at 1540 and 1168 cm^{-1}. The peaks at 2939 cm^{-1} and 2873 cm^{-1} correspond to the asymmetric stretching vibration and symmetric stretching vibration of the methylene respectively. Notably, the absorbance of isocyanate groups at approximately 2270 cm^{-1} was absent in spectrum, indicating the successful preparation of DLPU. The FT-IR spectrum of GelMA was shown in Fig. 2. It exhibited absorbance from 3411 to 3289 cm^{-1} confirming the presence of peptide bonds (mainly N–H stretching) [38]. The obvious absorbance peak at 1645 cm^{-1} could be assigned to C═O stretching vibration, and the peak at 1531 cm^{-1} was assigned to C–N stretching plus N–H bending. The high hydrophilicity could be anticipated from the abundant amino and amide groups of GelMA [30].

Fig. 2b and c reveal the ^{1}H NMR of the DLPU and GelMA. The structure of DLPU was characterized and analyzed using ^{1}H NMR spectroscopy [11]. Illustrating in Fig. 2b, the obvious peak at 4.05 ppm was attributed to the CH$_2$ group in the structure of DMPA. The peak at 3.51 ppm was assigned to the CH$_2$ group in IPDI as well as PEG, which coincides with mentioned in literature [39]. The observed signal peak at 7.12 ppm was attributed to the N–H group of amide group. The chemical shift value of about 1.4 ppm belongs to the CH$_3$ in the structure of IPDI and DMPA [11]. The DS is a significant factor in impacting on the mechanical properties of GelMA and the G-DLPUs as well. The ^{1}H NMR spectroscopy of GelMA was characterized to assess the DS of GelMA, which was calculated quantified using equation (1) and the calculated result is 87.6%.

Furthermore, to reveal the interaction of composite materials, zeta potential was used to measure the potential of the solution G-DLPUs, and the results were shown in Fig. 2d. The zeta potential values are −10.50 mV, −32.3 mV, −27.14 mV, −22.44 mV, and −13.74 mV for GelMA, DLPU, G-DLPU3, G-DLPU2, and G-DLPU1, respectively. The values of zeta potential illustrated that the electrostatic repulsive energy of particles in solution is reduced, which suggests the electrostatic interaction existed between DLPU and GelMA in G-DLPUs.

3.1.2. Rheological properties

The mechanical properties of hydrogel play a critical role in its clinical application. The mechanical strength and gelation mechanism of hydrogels were analyzed using rheometer.

The amplitude sweep results provided the storage modulus (G′), and the extent of hydrogen bond and covalent bond formation between DLPU and GelMA can be indicated by the G′. Fig. 3a showed the measurements (G′) of the different samples. With the mixing of DLPU and GelMA and the formation of a dual network structure, the mechanical strength of hydrogel increased significantly from 628 Pa to 1332 Pa due to the increasing density of crosslinking network (shown in Fig. S4).

Furthermore, the sol–gel transition behavior of G-DLPU3 was conducted using a rheometer at a fixed frequency (1 Hz) and 1% strain with the intermittent irradiation of UV light. As shown in Fig. 3b, at the initial stage the storage moduli (G′) was very low. Subsequently, with increased UV exposure time, a significant increase in G′ was observed, revealing the sol–gel transition. Longer UV exposure time led to the enhanced modulus due to the formation of denser network structure shown as Fig. S4. For composite irradiated by UV for 1, 2 and 3 min, the storage moduli (G′) of the complex was 1450, 4230, and 6130 Pa, respectively.

3.1.3. The SEM images and water contact angle of hydrogels

The surface topography of the materials is shown in Fig. 3c. Poly-urethane hydrogel is smooth after drying and just a few of fibrous tubes could be observed on surface due to it contains softer segments such as PEG400. However, large amount pores could be observed in the GelMA, which allow cell adhesion and proliferation. While, the pore of GelMA is unstable and fragile. Because of the electrostatic attraction and the hydrogen bonding interaction of the DLPU and GelMA, the structure of G-DLPU became denser and neater, which could maintain the stability of the pore and network structure in the hydrogel. It is obvious to make the conclusion that introducing GelMA in DLPU matrix could contribute to maintaining the 3D porous structure and endow the composite porous surface. Compared with DLPU, the G-DLPUs with three-dimensional porous structure allows the interchange of body fluid and maintains moisture around wound.

The hydrophilicity of samples was evaluated by measuring the surface contact angle, which strongly reflected the liquid-absorption capacity and the adhesion for cell on the materials. Fig. 3d shows the results of different samples in static water contact angle. The samples of GelMA, DLPU, G-DLPU1, G-DLPU2 and G-DLPU3 show water contact angle of 33.86 ± 5.54°, 66.47 ± 3.25°, 58.91 ± 4.61°, 45.37 ± 4.46° and 39.26 ± 4.73° respectively, indicating that all the samples were hydrophilic due to the static water contact angles in all samples were lower than 90°. The water contact angle decreased with the increase ratio of GelMA, exhibiting the significant improvement in hydrophilicity, which result from the increase density of active hydrophilic groups such as hydrophilic amino and carboxyl groups. The improvement of G-DLPUs in hydrophilicity would be greatly promote the performance of degradability and biocompatibility.

3.1.4. Water absorption and water retention ability

The water-absorption capability of adhesive plays a vital role in absorbing exudate from wound. Fig. 3e illustrates that DLPU shown a liquid-absorption rate of up to 51%, which could be attributed to the fact that DLPU contains luxuriant hydrophilic groups [37], such as carboxyl

groups.

Furthermore, the GelMA was reported recently to act as a plasticizer or container to increase hydrogel in liquid-absorption capacity and liquid-holding capacity, owing to its excellent water-soluble ability [23]. Comparing with DLPU, the stability of G-DLPUs in water uptake and retention has been significantly improved, as shown in Fig. 3f and Figs. S1 and S2, which would be attributed to the enrichment of hydrophilic groups in G-DLPUs [11]. The outstanding performance of G-DLPUs in absorb exudate is attributed to the porous three-dimensional structure, liquid-absorption capacity and standout liquid holding property, make it outstanding competitor in the field of wound closure.

3.2. Mechanical behavior

The mechanical properties of the adhesive have a great impact on achievements of shape-adaptive adhesion. The representative stress-strain curves of the G-DLPUs are shown in Fig. 4. Having the maximum tensile strength, the G-DLPU3 shows its elongation at break more than 200%. While, the GelMA is fragile and shows an extremely limited stretching ability, which might produce fragments after collapse in body, and further block blood vessels or damage the surrounding tissues, unpredictably. In addition, comparing with the GelMA, the G-DLPU1 displayed higher strength in stretching and longer elongation at break. The tensile strength of G-DLPU1, G-DLPU2 and G-DLPU3 was 71.37 kPa, 83.52 kPa and 127.42 kPa with the elongation at break of 111.16%, 145.28% and 203.30%, respectively (Fig. 4b). The detailed data shown in Fig. 4c and Table S1. In addition, the elongation at break displayed that G-DLPUs possesses stable tensile properties. Moreover, the cyclic tensile properties of G-DLPUs were further evaluated, and the results were shown in Fig. 4d, which illustrated that the G-DLPUs possesses good flexibility and fatigue resistance.

When the tissue adhesive is used in vivo, it will inevitably be compressed and deformed by the surrounding tissues. So, it is particularly important to evaluate the stability of the tissue adhesive in mechanical properties. The typical curves and the summary of G-DLPUs in compression performance shown in Fig. 4f and Table S2, depict that the sample containing more DLPU trends to possess a high compressive strength, even up to 80 kPa, that reveals the G-DLPU3 has good structural stability and pressure resistance. In addition, after cyclic compression tests, the stress of the G-DLPU3 did not decrease, showing excellent fatigue resistance (Fig. 4g and h).

Obviously, with the increase of DLPU content, the elongation at break, tensile strength and compressive strength including fatigue resistance of G-DLPUs were evidently strengthen, due to the DLPU segments containing carboxyl and other groups, which enhance the interaction between DLPU and GelMA via electrostatic and hydrogen bonding interaction, shown in Fig. 1. Preventing high modulus tissue adhesive from scratching tissues during wound recovery, the G-DLPUs was also endowed with appropriate tissue shape adaptability. Thus, the G-DLPUs containing amino acid-rich polyurethane presents a promising candidate for adhesive applicable in tissue engineering field.

3.3. Adhesive properties of hydrogels

In vitro porcine skin adhesion experiments were performed to evaluate the tissue adhesion strength of G-DLPUs. The schematic diagram of shear strength and tensile strength are illustrated in Fig. 5a and d respectively. In addition, the summary of G-DLPUs in adhesion performance shown in Table S3 and Table S4. The representative curve of G-DLPUs in shear strength (shown in Fig. 5b) and the mean and error bars (shown in Fig. 5) clearly exhibit that the shear strength of GelMA and G-DLPUs shows the law of increasing successively in value with the increasing of DLPU content. The representative curve of G-DLPUs in tensile strength to porcine skin (depicted in Fig. 5e) and the mean and error bars (displayed in Table S4), display the value of tensile strength of G-DLPUs could reach to more than 100 kPa. The tensile adhesion

performance of G-DLPUs to skin (inner and outer surface) were shown in Fig. 5f. The realization of high adhesion strength is attributed to the fact that the DLPU and GelMA molecular chain contain a great quantity of carboxyl groups and amino groups that can form the interaction with skin tissues by the form of hydrogen bonds [4,21,40]. The developed G-DLPUs composites can have promising applications in tissue adhesion to close wounds. This strong hydrogen bond interaction with G-DLPUs is also shown in the adhesion to glass, metal and plastic which exhibited in Fig. 5 and Movies S1, S2 and S3. Holding great potential to adhere to the tissue, the G-DLPUs exhibit auspicious for tissue adhesiveness making the tissue adhesion boost the application in more related fields.

Supplementary video related to this article can be found at https://doi.org/10.1016/j.bioactmat.2022.01.009

3.4. Biodegradation evaluation in vitro

The biocompatibility and controllability of degradation are significant in the biomedical field, including tissue adhesives. For the materials used in tissue adhesives, except for the adhesion strength, the degradation properties involving the pH value, the mass loss and the biocompatibility of the biodegradation solution are also critical.

To simulate the degradation environment in vivo, we investigated the hydrolytic degradation property of G-DLPUs in PBS containing collagenase. It is displayed from Fig. 6b that the GelMA had a rapid degradation process that could completely degraded within 20 days, which may not conducive to the healing and recovery of the wound. While, during 90 days of degradation, the remaining mass of the DLPU and G-DLPU3 decreased gradually, and the mass loss reached 66.56% and 93.26% respectively. That indicated the formation of uniform dual network structure with GelMA in G-DLPUs adhesive hydrogel could significantly improve the degradability of DLPU.

Fig. 6c demonstrates the pH value of the biodegradation liquid of G-DLPUs degrading in PBS (initial pH = 7.4). The pH value of DLPU and G-DLPUs' degradation solutions vary between 7.0–7.4, while, DSP' degradation was as low as 4.0, which exhibiting potential non-negligible tissue toxicity [11,26].

FT-IR was used to investigate chemical structure before and after degradation of DLPU for 1, 2 and 3 months, and the results were shown as Fig. 6d. From the spectrum, it can be observed that the peak present at 3368 cm^{-1} became broader with the degradation time increases to 2 months and 3 months, that could associate with the absorption peak of the hydroxyl and amino groups after degradation. Moreover, the absorption peak at 1730 cm^{-1} attributing to the ester carbonyl group was drastically decreased, suggesting that the biodegradation and hydrolysis reactions of the polyester molecular chains occurred.

The differential scanning calorimetry (DSC) was applied to analyze the microphase structure of the DLPU during the degradation. The glass transition temperature (T_g) of DLPU demonstrating in Fig. 6e was significantly shifted to high temperature, indicating the reaction of biodegradation occurred in the soft-segment amorphous region having been proven in the previous report [11]. Detailly, the soft segment has higher rearrangement ability and motility, which could make it easier for soft segment to achieve glass transition after undergoing the degradation process [41], and schematic representation of the biodegradation process of DLPU was shown in Fig. 6a.

3.5. Biocompatibility evaluation in vitro

It is significant to evaluate the growth of cells on materials, because it can provide reliable and effective data for in vivo clinical trials and provide guidance for practical applications. The spreading degree and distribution density of cells on hydrogels are presented in Fig. 7a, which displayed both the fluorescence micrographs and statistics. All the samples could support the adhesion and growth of cells as Fig. 7 shows. It is shown that higher densities and larger areas of spreading for cells to adhere on G-DLPU3, GelMA than on DSP, and DLPU surfaces. While, it

displays the lowest spreading and adhering density of cells on DSP. The reason for the cells exhibiting vigorous growth behaviors on surfaces of samples is that the G-DLPUs possess excellent biocompatibility which could provide a pleasurable environment for cells to adhere and grow as shown in Fig. 7a. The excellent biocompatibility of G-DLPUs may attribute to the existence of functional groups of the urethane and amino acids, which have been proven that this groups could act function as potential cell adhere sites and have active impact on cell growth [42]. On the contrary, the poor biocompatibility of DSP, would inevitably cause the increase of the concentration of toxic substances, which eventually resulted in the apoptosis.

The hemolysis test can be applied to assess the blood cell compatibility of the material (shown in Fig. 7d and e). After the centrifugation, the positive control was found to be clarified red and there was no red blood cells reside at the bottom of the tube. The red blood cells precipitated at the bottom in all tubes of GelMA, DLPU, G-DLPUs and the negative control, besides, the supernatant was colorless and clarified, indicating no hemolysis effect. Quantitatively, the hemolysis rate of the GelMA, DLPU and G-DLPUs was 0.65%, 3.16%, 1.80%, 1.98% and 2.68%, respectively, which was far less than 5%, indicating that all materials had no hemolytic effect [23] (Fig. 7e). Therefore, it is proved from the hemolysis test that DLPU and G-DLPUs did not affect red blood cells when in contact with blood.

The evaluation for the biocompatibility of the degradation liquid could objectively reflect the biological toxicity of the material to the surrounding tissues during the degradation process in vivo. In this study, the cell viability in degradation solution of the G-DLPUs was measured by the CCK-8 assay using the pre-determined-time degradation solution mixed with DMEM. It was proved that the degradation products of DLPU almost had no cytotoxicity from the results of the CCK-8 assay, which displayed not significant difference between the DLPU and control group during 3 months in the absorbance values. However, comparing with the control group, the DSP degradation products had significant cytotoxicity on cell proliferation, due to the absorbance values were obviously lower than that of the control group. In addition, the rapid and uncontrollable degradation of DSP (shown in Fig. 6.), makes the concentration of COOH in solution rise sharply and lower the pH of solution, which would be promoted the apoptosis of the cell. On the contrary, modified by DMPA and amino acid, the DLPU has a controllable and gentle degradation process, and its excellent biocompatibility could provide a comfortable environment for cells to adhesion and growth. Besides, DLPU possesses excellent and long-acting cell biocompatibility the conclusion can be obtained from the analysis of Fig. 7. The biodegradation of GelMA will be decomposed into many polypeptides and beneficial amino acids, especially, the RGD polypeptide chain, which has been reported to promote wound tissue repair. The biocompatibility of G-DLPU3 is strengthened after combining DLPU with GelMA, therefore, the G-DLPUs are expected to improve the rate of wound healing.

3.6. The NO generation in vitro

Due to the crucial role of L-Arg in the wound healing process, the release behavior of L-Arg during the in vitro degradation process was measured. The standard curve and the measured absorbance intensity were shown in Fig. S7a, it could be known that the releasing behavior of L-Arg in the G-DLPU3 was cumulatively calculated to be 1.03%, 1.54% and 1.97%, and the release amount can reach 4.36% within 7day (Fig. S7b). It demonstrates that the L-Arg could be released stably in G-DLPU3 when treated the wound, which is advantageous to promoting wound healing.

The generation of NO during the L-Arg release was studied via incubating the HUVECs with G-DLPU3 degradation liquid. Then, after employing the NO-sensitive fluorescent probe diaminofluorescein-FM diacetate (DAF-FM DA), the NO production could be measured using fluorescence microscopy. The generated NO was measured by quantifying the intensity of fluorescence in captured images. After 15 min of

incubation with the degradation liquid, the enhancement of bright green fluorescence was observed (Fig. 8a and b). After reaching the peak at 60 min, the intensity of fluorescence gradually decreased subsequently.

The Griess reaction was used to monitor the nitrite level in the supernatant of G-DLPU3-exposed cell culture according to the operation manual. The result of normalized relative nitrite levels was shown in Fig. 8c. Compared with the 0.1 μM concentration before the addition of degradation liquid, the absolute nitrite level was markedly increased after being incubated for 180 min (0.43 μM), which indicated that NO was continuously released from cells, that would enhance the promotion of angiogenesis during use in vivo [36].

3.7. Hemostasis and wound healing

Prior to verifying the in vivo wound healing and hemostatic effect, the in vivo biocompatibility of the material was evaluated by carrying out a subcutaneous implantation experiment in rat. It was demonstrated that the hydrogel decreased gradually in rat body, tightly adhered to the implantation site and did not show swelling, redness and bleeding, indicating good biocompatibility and excellent degradation safety of these hydrogels (Fig. S3).

The macroscopic diagram of the adhesion firmness of G-DLPU3 after 3 h; (h) H&E staining of liver sections from G-DLPUs group (magnification: 400 ×, scale bar: 100 μm); (i) Normal group.

Based on excellent biocompatibility in vitro and in vivo, and strong adhesion, in vivo adhesion hemostasis performance of G-DLPUs was further evaluated using the rat hemorrhaging liver model [26]. Adhering firmly to a physical hemorrhage site, the adhesive hydrogel (G-DLPU3) could rapidly help form a hemostatic barrier as shown in Fig. 9. From the results, it could be found that, the prepared tissue adhesive shows excellent wound closure and hemostatic properties, because the total blood loss of the untreated group is averagely 1.015 g, whereas blood loss in the G-DLPU3-treated groups was just only 0.289 g. It was observed that the statistical differences (p < 0.05) between untreated and G-DLPU3-treated group that means the G-DLPUs possess excellent tissue adhesion properties and have promising prospect for further employed as hemostatic adhesive in the field of trauma.

The rats survived and then gradually started to move after 3–6 h. The liver was reddish brown and there was no exudation and suppuration observed in the incision of the wound after removing the tissue adhesive. The histological analysis of samples taken after 3 h of adhesion to the liver is shown in Fig. 9. Then the liver tissue of rat was fixed by immersing in 10% buffered formalin immediately. Subsequently, the samples were processed in the order of paraffin embedding, sectioning and deparaffinization, and performed H&E staining following standard steps at last. There were no significant changes in cell morphology compared with the normal group, besides, there was no obvious inflammatory cell infiltration and tissue necrosis, especially no neutrophils observed around the tissue, indicating that the samples almost have no affects to the liver [43,44]. This clearly indicates that the G-DLPUs possess excellent biocompatibility and effective hemostasis, would be expected to use as a hemostatic patch for hemostasis of internal organs.

To assess the effects of G-DLPU3 on wound healing and blood vessel regeneration in wound, a full-thickness skin defect model was used (Fig. 10). Fig. 10b shows typical images of the wounds during the healing process, showing that wound areas in all groups gradually decreased over time (Fig. 10b). After treatment for 7 days, wounds treated with G-DLPU3 showed significantly accelerated wound healing with 67.3% wound closure, respectively, were higher than the control group (36.8%). On day 14, the control group displayed unclosed wound areas of 27.9%. In contrast, no obvious wounds were observed in the G-DLPU3 treated group, with mouse showing a degree of hair coverage. The significantly improved wound healing effects of the G-DLPU3 compared with control may be ascribed to the ability of the adhesion of G-DLPU3 to provide a moist recovery environment for the wound.
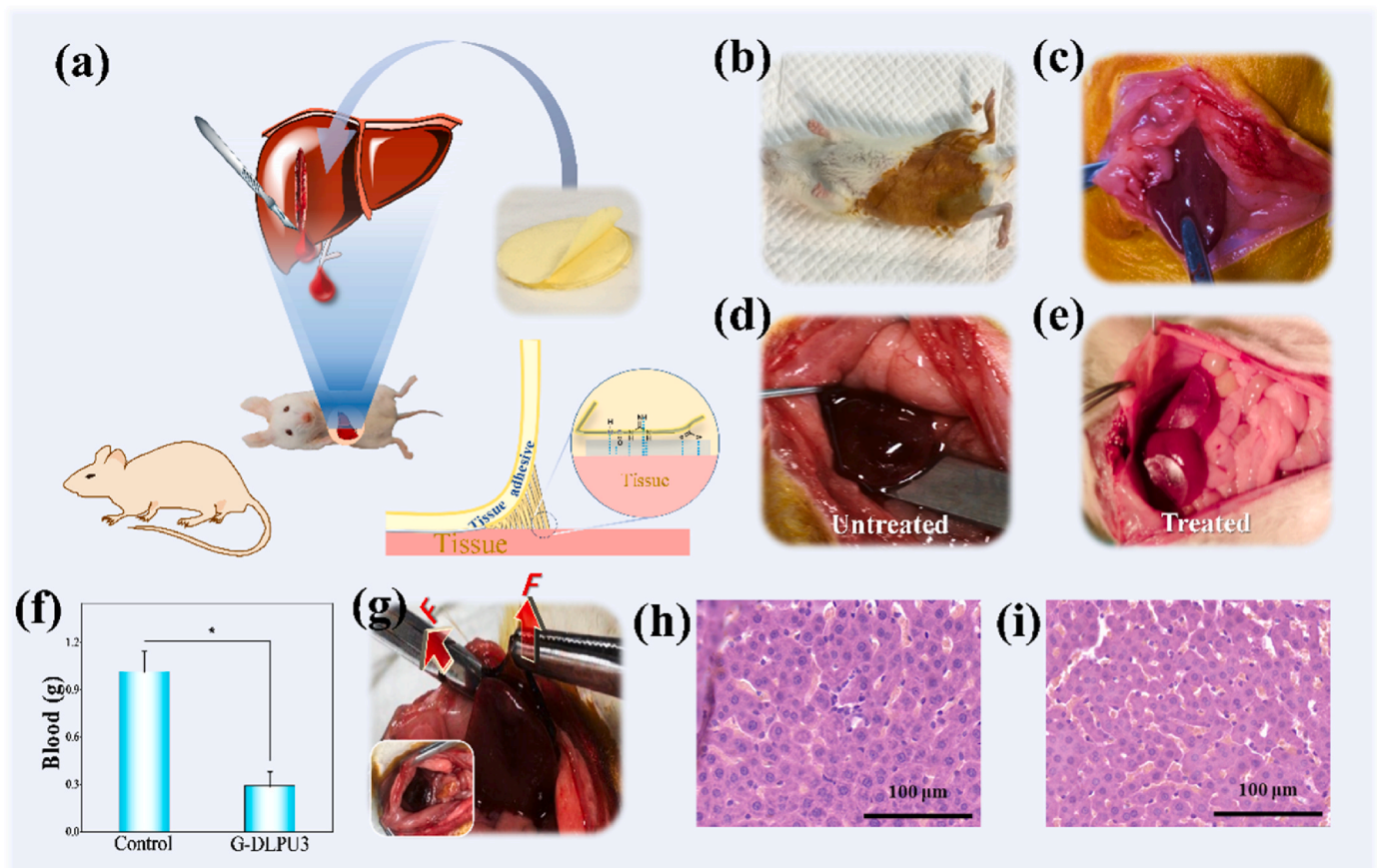
Fig. 9. Wound adhesion evaluation in vivo. (a) Schematic diagram of the adhesion effect of G-DLPU3 on damaged liver of rat.; (b) Anesthetized rat; (c) Exposed liver; (d) Damaged liver tissue of rat (untreated); (e) The damaged liver tissue treated with G-DLPU3; (f) Total blood loss (n = 3). Error bars, mean ± s.d. *p < 0.05, represents significant difference compared with blank group; (g).

Moreover, the L-Arg and RGD released during the degradation of G-DLPU3 played a vital role in the recovery process.

To further investigate the wound healing performance of G-DLPUs, the H&E staining on the regenerated skin were performed at 3rd, 7th, and 14th days, and the results were shown in Fig. 10. At the 3rd day, number of inflammatory cells (neutrophils, marked with red arrows) could be observed in both experimental group and control group, while, the G-DLPUs treated group exhibited fewer inflammatory cells compared to the control group. After 7- and 14-day treating, the inflammatory cells fade away and fibroblasts (marked with blue arrows) gradually appeared, especially in the G-DLPUs group [45]. The results indicated that G-DLPUs just caused extremely slight inflammatory reaction compared with the control group, which likely attributed to the release of L-Arg and the ability of G-DLPUs hydrogel to isolate the wound from the external environment [2].

Vascularization of the wound tissue is one of important symbols of wound healing. The immunohistochemical staining of CD31, a marker of endothelial cells, was characterized and evaluated in this study. The results displayed that compared with the CD31 positive staining found in the blank group (Fig. 10d), it is more and obvious CD31 positive staining was observed in the wound tissue treated by the G-DLPUs group. The quantitative analysis (Fig. 10e and f) showed that the G-DLPUs group had a high neovascularization on the 7th and 14th days due to the release of L-Arg from G-DLPUs. However, the amount of appeared angiogenesis is significantly less in the control group. Furthermore, on 14th day, the G-DLPUs group produced larger blood vessels (Fig. 10f), which would provide wound tissue more nutrition during wound healing. Besides, compared with the control group on the 7th and 14th day, the G-DLPUs group showed thicker epidermis

(Fig. 10d). The result would be largely attributed to the fact that the L-Arg and RGD released during the degradation of the wound adhesive could promote the adhesion and proliferation of vascular endothelial cells, and ultimately accelerate tissue repair. Instead of complicated steps for wound care such as injection or light curing around the wound [2], the G-DLPUs adhesive could be firmly adherent to wound bed and exert therapeutic effect. It is highlighted the G-DLPUs hydrogel as promising wound adhesive that can adhere to the moist in vivo wound environment and promote wound healing.

4. Conclusions

Hemostasis and promotion of angiogenesis are two crucial problems related to tissue damage. The bioactive wound adhesive constructed in this study addressed problems due to its function of both efficient hemostasis and enhancing tissue healing attributing to the release of L-Arg and the strong tissue adhesion ability. Hence, we constructed the multifunctional adhesive (G-DLPUs) by compounding GelMA with bio-based polyurethane (DLPU), which possesses excellent adhesion and could release L-Arg during its degradation process. This double-network-structure hydrogel adhesive would absorb exudates from the wound with porous structure and form the strong adhesion at the interface of skin and liver to promote rapid hemostasis, which was further verified by in vivo hemostatic experiments. Besides, the degradation process of G-DLPUs had excellent biocompatibility which was proven via in vitro experiment and in vivo subcutaneous implantation experiment. Moreover, having the capacity to generate NO, the synergistic bioactivity of L-Arg and RGD released from the wound adhesive during the degradation process could help to achieve wound healing
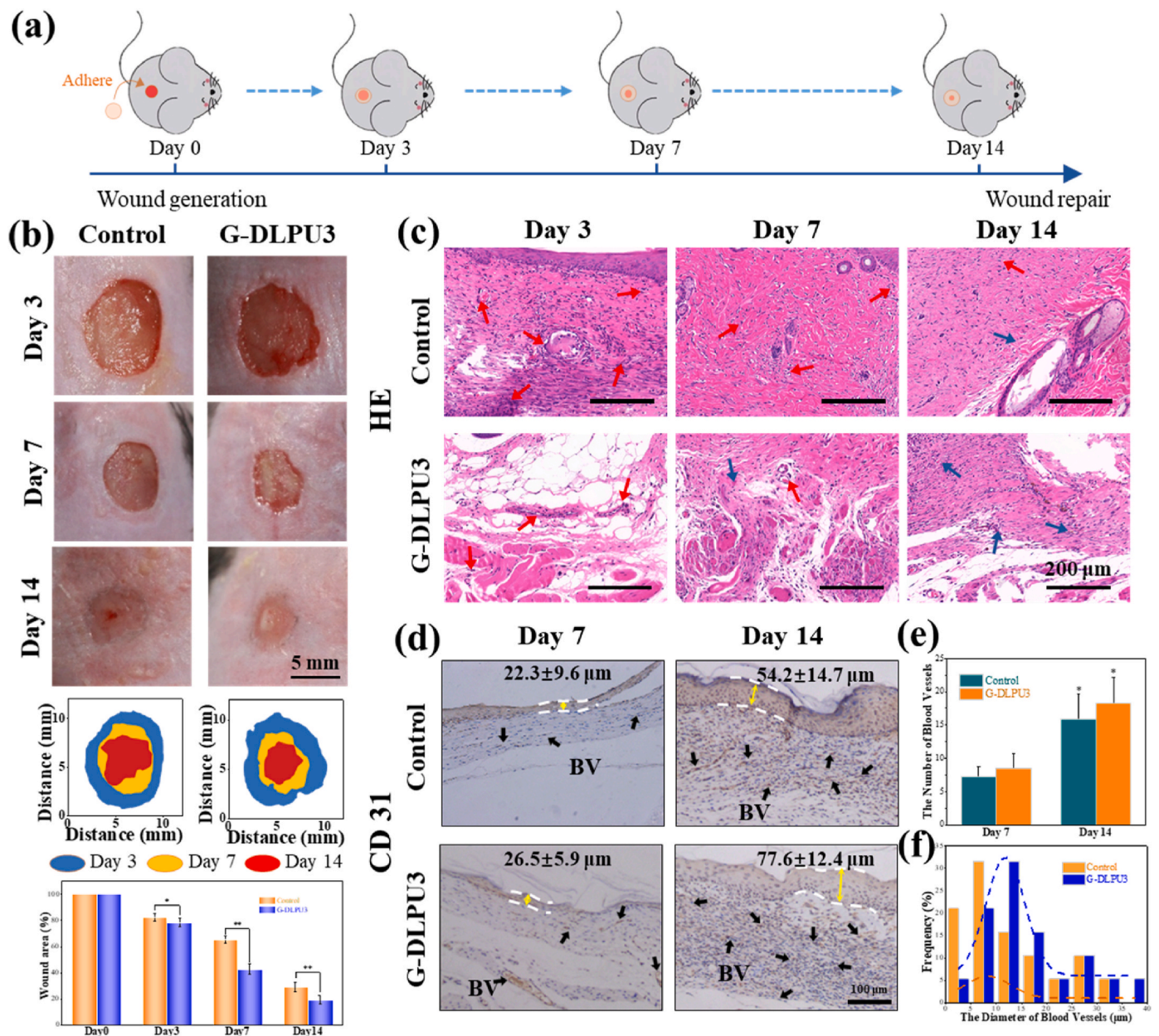
Fig. 10. In vivo biocompatibility evaluation of G-DLPU3; (a) Schematic diagram of wound healing experiment; (b) Representative wound images after treated for 3 days, 7days and 14 days and the area traces of wound closure during 14 days (n = 3). Error bars, mean ± s.d. *p < 0.05, **P < 0.01, represents significant difference compared with control group; (c) H&E staining of the wound tissues from each treatment group at 3, 7, and 14 days (fibroblasts: blue arrows, neutrophils: red arrows. scale bar: 200 μm). (d) Images of immunohistochemical staining for CD31 on the 14th day (BV, blood vessels; boundary of epithelium: white lines. scale bar: 100 μm). (e) Number blood vessels of the 14th day (n = 3). Error bars, mean ± s.d. *p < 0.05, represents significant difference compared with blank group. (f) Vessel diameter distribution on the 14th day. (For interpretation of the references to color in this figure legend, the reader is referred to the Web version of this article.)

through enhancing the regeneration of blood vessel, which was further proved using a mouse full-thickness skin defect model. Furthermore, this composite hydrogel can act as a pioneer to construct multifunctional tissue adhesive, providing solutions and inspiration for new type of tissue adhesive.

CRediT authorship contribution statement

Faxing Zou: Conceptualization, Investigation, Methodology, Writing – review & editing. **Yansen Wang:** Supervision, Validation, grammar revision. **Yudong Zheng:** Resources, Validation, Supervision. **Yajie Xie:** Methodology, Investigation. **Hua Zhang:** Methodology, Investigation. **Jishan Chen:** Data curation, Visualization. **M.Irfan**

Hussain: Investigation. **Haoye Meng:** Visualization. **Jiang Peng:** Resources, Supervision.

Declaration of competing interest

The authors declare that they have no known competing financial interests or personal relationships that could have appeared to influence the work reported in this paper.

Acknowledgements

Appendix A. Supplementary data

Supplementary data to this article can be found online at https://doi.org/10.1016/j.bioactmat.2022.01.009.

References

[1] G.C. Gurtner, S. Werner, Y. Barrandon, M.T. Longaker, Wound repair and regeneration, Nature 453 (7193) (2008) 314–321.

[2] L. Wang, X.H. Zhang, K. Yang, Y.V. Fu, T.S. Xu, S.L. Li, D.W. Zhang, L.N. Wang, C. S. Lee, A Novel double-crosslinking-double-network design for injectable hydrogels with enhanced tissue adhesion and antibacterial capability for wound treatment, Adv. Funct. Mater. 30 (1) (2020).

[3] K.E. Rudd, J.S. Charlotte, K.M. Agesa, S.K. Anne, T. Derrick, K.D. Rhodes, D. V. Colombara, K.S. Ikuta, K. Niranjan, F. Simon, Global, regional, and national sepsis incidence and mortality, 1990-2017: analysis for the Global Burden of Disease Study, Lancet (London, England) 395 (10219) (2020) 200–211.

[4] Z. Ahmadian, A. Correia, M. Hasany, P. Figueiredo, F. Dobakhti, M.R. Eskandari, S. H. Hosseini, R. Abiri, S. Khorshid, J. Hirvonen, H.A. Santos, M.A. Shahbazi, A hydrogen-bonded extracellular matrix-mimicking bactericidal hydrogel with radical scavenging and hemostatic function for pH-responsive wound healing acceleration, Adv. Healthc. Mater. 10 (3) (2021) 19.

[5] B.L. Guo, R.N. Dong, Y.P. Liang, M. Li, Haemostatic materials for wound healing applications, Nat. Rev. Chem. 5 (11) (2021) 773–791.

[6] C. Ghobril, M.W. Grinstaff, The chemistry and engineering of polymeric hydrogel adhesives for wound closure: a tutorial, Chem. Soc. Rev. 44 (7) (2015) 1820–1835.

[7] H.H. Versteeg, J.W.M. Heemskerk, M. Levi, P.H. Reitsma, New fundamentals in hemostasis, Physiol. Rev. 93 (1) (2013) 327–358.

[8] C.H. Dreyer, K. Kjaergaard, M. Ding, L. Qin, Vascular endothelial growth factor for in vivo bone formation: a systematic review, J. Orthop. Translat. 24 (2020) 46–57.

[9] M. Li, Y.P. Liang, J.H. He, H.L. Zhang, B.L. Guo, Two-pronged strategy of biomechanically active and biochemically multifunctional hydrogel wound dressing to accelerate wound closure and wound healing, Chem. Mater. 32 (23) (2020) 9937–9953.

[10] W. Zhang, T.J. Ji, S. Lyon, M. Mehta, Y.Q. Zheng, X.R. Deng, A.D. Liu, A. Shagan, B. Mizrahi, D.S. Kohane, Functionalized multiarmed polycaprolactones as biocompatible tissue adhesives, ACS Appl. Mater. Interfaces 12 (15) (2020) 17314–17320.

[11] Z.X. Feng, D. Wang, Y.D. Zheng, L. Zhao, T. Xu, Z.M. Guo, M.I. Hussain, J.S. Zeng, L.Y. Lou, Y. Sun, H.Y. Jiang, A novel waterborne polyurethane with biodegradability and high flexibility for 3D printing, Biofabrication 12 (3) (2020) 16.

[12] K. Hristina, T. Langerholc, M. Trapecar, Novel metabolic roles of L-arginine in body energy metabolism and possible clinical applications, J. Nutr. Health Aging 18 (2) (2014) 213–218.

[13] A. Zl, D.A. Jing, B. Zz, B. Hs, B. Ws, Y.A. Bo, L.A. Hai, Y.A. Xiao, A. Jc, A. Xz, Spatiotemporal manipulation of L-arginine release from bioactive hydrogels initiates rapid skin wound healing accompanied with repressed scar formation, Appl. Mater. Today. 24 (2021) 101116.

[14] B. Leigh, K. Desneves, J. Rafferty, L. Pearce, S. King, M.C. Woodward, D. Brown, R. Martin, T.C. Crowe, The effect of different doses of an arginine-containing supplement on the healing of pressure ulcers, J. Wound Care 21 (3) (2012) 150–156.

[15] M. He, A. Potuck, Y. Zhang, C.C. Chu, Arginine-based polyester amide/polysaccharide hydrogels and their biological response, Acta Biomater. 10 (6) (2014) 2482–2494.

[16] J.E. Park, M.J. Abrams, P.A. Efron, A. Barbul, Excessive nitric oxide impairs wound collagen accumulation, J. Surg. Res. 183 (1) (2013) 487–492.

[17] L. Zhou, H. Zheng, Z. Liu, S. Wang, Z. Liu, F. Chen, H. Zhang, J. Kong, F. Zhou, Q. Zhang, Conductive antibacterial hemostatic multifunctional scaffolds based on $Ti_3C_2T_x$ mxene nanosheets for promoting multidrug-resistant bacteria-infected wound healing, ACS Nano 15 (2) (2021) 2468–2480.

[18] M. Movahedi, A. Asefnejad, M. Rafienia, M.T. Khorasani, Potential of novel electrospun core-shell structured polyurethane/starch (hyaluronic acid) nanofibers for skin tissue engineering: in vitro and in vivo evaluation, Int. J. Biol. Macromol. 146 (2020) 627–637.

[19] K.C. Hung, C.S. Tseng, L.G. Dai, S.H. Hsu, Water-based polyurethane 3D printed scaffolds with controlled release function for customized cartilage tissue engineering, Biomaterials 83 (2016) 156–168.

[20] H. Zebiri, H. van den Berghe, S. Sayegh, P.E. Chammas, C. Pompee, M. Chammas, X. Garric, Synthesis of PLA-poly(ether urethane)-PLA copolymers and design of biodegradable anti-adhesive membranes for orthopaedic applications, J. Mater. Chem. B 9 (3) (2021) 832–845.

[21] S. Balcioglu, H. Parlakpinar, N. Vardi, E.B. Denkbas, M.G. Karaaslan, S. Gulgen, E. Taslidere, S. Koytepe, B. Ates, Design of xylose-based semisynthetic

[22] Z.X. Feng, Y.D. Zheng, L. Zhao, Z.Y. Zhang, Y. Sun, K. Qiao, Y.J. Xie, Y.S. Wang, W. He, An ultrasound-controllable release system based on waterborne polyurethane/chitosan membrane for implantable enhanced anticancer therapy, Mater. Sci. Eng. C-Mater. Biol. Appl. 104 (2019) 109944.

[23] C. Cui, W. Liu, Recent advances in wet adhesives: adhesion mechanism, design principle and applications, Prog. Polym. Sci. 116 (2021) 101388.

[24] Y. Hong, F. Zhou, Y. Hua, X. Zhang, H. Ouyang, A strongly adhesive hemostatic hydrogel for the repair of arterial and heart bleeds, Nat. Commun. 10 (1) (2019) 11.

[25] I. Strehin, Z. Nahas, K. Arora, T. Nguyen, J. Elisseeff, A versatile pH sensitive chondroitin sulfate–PEG tissue adhesive and hydrogel, Biomaterials 31 (10) (2010) 2788–2797.

[26] H. Yuk, C.E. Varela, C.S. Nabzdyk, X. Mao, R.F. Padera, E.T. Roche, X. Zhao, Dry double-sided tape for adhesion of wet tissues and devices, Nature 575 (7781) (2019) 169–174.

[27] K. Yue, X.Y. Li, K. Schrobback, A. Sheikhi, N. Annabi, J. Leijten, W.J. Zhang, Y. S. Zhang, D.W. Hutmacher, T.J. Klein, A. Khademhosseini, Structural analysis of photocrosslinkable methacryloyl-modified protein derivatives, Biomaterials 139 (2017) 163–171.

[28] Y.T. Zheng, G. Wu, L.M. Chen, Y. Zhang, Y.W. Luo, Y. Zheng, F.J. Hu, T. Forouzanfar, H.Y. Lin, B. Liu, Neuro-regenerative imidazole-functionalized GelMA hydrogel loaded with hAMSC and SDF-1 alpha promote stem cell differentiation and repair focal brain injury, Bioact. Mater. 6 (3) (2021) 627–637.

[29] Y. Cao, S. Yang, D. Zhao, Y. Li, S.S. Cheong, D. Han, Q. Li, Three-dimensional printed multiphasic scaffolds with stratified cell-laden gelatin methacrylate hydrogels for biomimetic tendon-to-bone interface engineering, J. Orthop. Translat. 23 (2020) 89–100.

[30] H. Shirahama, B.H. Lee, L.P. Tan, N.J. Cho, Precise tuning of facile one-pot gelatin methacryloyl (GelMA) synthesis, For. Rep. 6 (2016) 31036.

[31] Y.S. Wang, C. Wang, Y.J. Xie, Y.Y. Yang, Y.D. Zheng, H.Y. Meng, W. He, K. Qiao, Highly transparent, highly flexible composite membrane with multiple antimicrobial effects used for promoting wound healing, Carbohydr. Polym. 222 (2019) 14.

[32] Y.S. Wang, Y.F. Zhao, L.X. Qiao, F.X. Zou, Y.J. Xie, Y.D. Zheng, Y. Chao, Y. Yang, W. He, S.M. Yang, Cellulose fibers-reinforced self-expanding porous composite with multiple hemostatic efficacy and shape adaptability for uncontrollable massive hemorrhage treatment, Bioact. Mater. 6 (7) (2021) 2089–2104.

[33] M.X. Chen, Z.X. Feng, W.M. Guo, D.J. Yan, S. Gao, Y.Y. Li, S. Shen, Z.G. Yuan, B. Huang, Y. Zhang, M.J. Wang, X. Li, L.B. Hao, J. Peng, S.Y. Liu, Y.X. Zhou, Q. Y. Guo, PCL-MECM-based hydrogel hybrid scaffolds and meniscal fibrochondrocytes promote whole meniscus regeneration in a rabbit meniscectomy model, ACS Appl. Mater. Interfaces 11 (44) (2019) 41626–41639.

[34] Y. Dai, H. Guo, L. Chu, Z. He, M. Wang, S. Zhang, X. Shang, Promoting osteoblasts responses in vitro and improving osteointegration in vivo through bioactive coating of nanosilicon nitride on polyetheretherketone, J Orthop Translat 24 (2020) 198–208.

[35] X. Huang, Q. Fu, Y.X. Deng, F.P. Wang, B. Xia, Z.M. Chen, G.B. Chen, Surface roughness of silk fibroin/alginate microspheres for rapid hemostasis in vitro and in vivo, Carbohydr. Polym. 253 (2021) 117256.

[36] M. Li, J. Li, J. Chen, Y. Liu, X. Cheng, F. Yang, N. Gu, Platelet membrane biomimetic magnetic nanocarriers for targeted delivery and in situ generation of nitric oxide in early ischemic stroke, ACS Nano 14 (2) (2020) 2024–2035.

[37] Y.S. Wang, C. Wang, L.X. Qiao, J.X. Feng, Y.D. Zheng, Y. Chao, W. He, Y.J. Xie, W. J. Shuai, M.L. Li, Shape-adaptive composite foams with high expansion and absorption used for massive hemorrhage control and irregular wound treatment, Appl. Mater. Today 13 (2018) 228–241.

[38] W.X. Weng, W.W. Wu, X.M. Yu, M.Y. Sun, Z.S. Lin, M. Ibrahim, H.Z. Yang, Effect of GelMA hydrogel coatings on corrosion resistance and biocompatibility of MAO-Coated Mg alloys, Materials 13 (17) (2020) 3834.

[39] S.H. Hsu, K.C. Hung, Y.Y. Lin, C.H. Su, H.Y. Yeh, U.S. Jeng, C.Y. Lu, S.H.A. Dai, W. E. Fu, J.C. Lin, Water-based synthesis and processing of novel biodegradable elastomers for medical applications, J. Mater. Chem. B 2 (31) (2014) 5083–5092.

[40] Z.C. Xu, L.T. Chen, L.L. Lu, R.C. Du, W.C. Ma, Y.F. Cai, X.M. An, H.M. Wu, Q. Luo, Q. Xu, Q.H. Zhang, X.D. Jia, A highly-adhesive and self-healing elastomer for bio-interfacial electrode, Adv. Funct. Mater. 31 (1) (2020) 9.

[41] X. Zhou, C. Fang, W. Lei, J. Su, L. Li, Y. Li, Thermal and Crystalline Properties of Waterborne Polyurethane by in situ water reaction process and the potential application as biomaterial, Prog. Org. Coating 104 (2017) 1–10.

[42] S.H. Pyo, P.R. Wang, H.H. Hwang, W. Zhu, J. Warner, S.C. Chen, Continuous optical 3D printing of green aliphatic polyurethanes, ACS Appl. Mater. Interfaces 9 (1) (2017) 836–844.

[43] S. Sangaletti, R. Ferrara, C. Tripodo, M.C. Garassino, M.P. Colombo, Myeloid cell heterogeneity in lung cancer: implication for immunotherapy, Cancer Immunol. Immunother. 70 (9) (2021) 2429–2438.

[44] Y.M. Khaw, C. Cunningham, A. Tierney, M. Sivaguru, M. Inoue, Neutrophil-selective deletion of Cxcr2 protects against CNS neurodegeneration in a mouse model of multiple sclerosis, J. Neuroinflammation 17 (1) (2020) 1–12.

[45] P. Wu, Y. Liang, G. Sun, Engineering immune-responsive biomaterials for skin regeneration, Biomater. Transl. 2 (1) (2021) 61–71.